Uterine DCs are crucial for decidua formation during embryo implantation in mice

Vicki Plaks,[1] Tal Birnberg,[2] Tamara Berkutzki,[3] Shay Sela,[4] Adi BenYashar,[2] Vyacheslav Kalchenko,[3] Gil Mor,[5] Eli Keshet,[4] Nava Dekel,[1] Michal Neeman,[1] and Steffen Jung[2]

[1]Departments of Biological Regulation, [2] Immunology, and [3]Veterinary Resources, The Weizmann Institute of Science, Rehovot, Israel.
[4]Department of Molecular Biology, Hadassah Hebrew University School of Medicine, Jerusalem, Israel.
[5]Department of Obstetrics, Gynecology and Reproductive Science, Yale University School of Medicine, New Haven, Connecticut, USA.

Implantation is a key stage during pregnancy, as the fate of the embryo is often decided upon its first contact with the maternal endometrium. Around this time, DCs accumulate in the uterus; however, their role in pregnancy and, more specifically, implantation, remains unknown. We investigated the function of uterine DCs (uDCs) during implantation using a transgenic mouse model that allows conditional ablation of uDCs in a spatially and temporally regulated manner. Depletion of uDCs resulted in a severe impairment of the implantation process, leading to embryo resorption. Depletion of uDCs also caused embryo resorption in syngeneic and T cell–deficient pregnancies, which argues against a failure to establish immunological tolerance during implantation. Moreover, even in the absence of embryos, experimentally induced deciduae failed to adequately form. Implantation failure was associated with impaired decidual proliferation and differentiation. Dynamic contrast-enhanced MRI revealed perturbed angiogenesis characterized by reduced vascular expansion and attenuated maturation. We suggest therefore that uDCs directly fine-tune decidual angiogenesis by providing two critical factors, sFlt1 and TGF-β1, that promote coordinated blood vessel maturation. Collectively, uDCs appear to govern uterine receptivity, independent of their predicted role in immunological tolerance, by regulating tissue remodeling and angiogenesis. Importantly, our results may aid in understanding the limited implantation success of embryos transferred following in vitro fertilization.

Introduction

Implantation is a critical stage in the establishment of pregnancy. Failure of the embryo to implant is clinically relevant to recurrent pregnancy loss and low success of in vitro fertilization. Despite some differences, the general principles of implantation are well conserved among mammalian species (1). Murine implantation starts with blastocyst apposition to the endometrium and attachment (E4–E4.5, vaginal plug is E0.5) that triggers the uterine stroma to proliferate and differentiate into the decidua, a spongy cell mass surrounding the blastocyst. Implantation then continues with the erosion of the epithelium that separates the blastocyst from the stroma, and embryonic trophoblasts invade the decidua and inner myometrium to reach maternal vessels. Decidualization is tightly associated with the spatial and temporal regulation of angiogenesis, i.e., the development of new capillaries from preexisting vessels (2). Angiogenesis at the implantation site (IS) is characterized by localized uterine vascular permeability along with the development of maternal vessels. With time, the latter dramatically increase in number and diameter in order to supply the fetal growing needs for oxygen and metabolites. The decidua supports the pregnancy, sustaining the embryo until the placenta is developed by E10. The decidua basalis, a remnant of the decidua at the implantation chamber will eventually be part of the outer side of the placenta, as it contacts the myometrium (3).

Approximately half of all human blastocyst implantations result in failed pregnancy. Multiple factors may contribute to this failure, including genetic or metabolic abnormalities of the embryo (4, 5). In addition, many of these early abortion cases are thought to result from poor uterine receptivity that, among other factors, may be associated with a maternal failure to immunologically tolerate the semiallogeneic embryo. Innate and adaptive immune responses in this unique environment are believed to be suppressed by the implanted embryo and the developing fetus during normal pregnancy (6). The key for a better understanding of this immunological tolerance probably resides within the decidual leukocyte populations. In both humans and mice, the most abundant hematopoietic cell type of the decidua are uterine NK cells (uNKs) (65%–70%). uNKs have been shown to be important in trophoblast migration and spiral artery transformation (7–9). However, they are believed to be dispensable for embryo implantation (9, 10). In addition, around 10%–20% of the decidual leukocyte population are MHC class II$^+$ (MHCII$^+$) APCs, whereas at least in humans, T cells are sparse and B cells are virtually absent (11). Among APCs, the most potent inducers of primary immune responses are CD11c^{hi} DCs, which represent around 5%–10% of all hematopoietic uterine cells (12). DC are a heterogeneous population of cells that initiate and coordinate the innate and adaptive immune responses. DCs are not only essential for the induction of primary immune responses but also important for the induction of immunological tolerance (13). Their function and stage of differentiation are regulated by the local microenvironment determined by cytokines and chemokines (14). Moreover, recent evidence points to a pivotal role of DCs in shaping the cytokine profile toward the establishment of a tolerogenic microenvironment at the maternal-fetal interface (15).

Nonstandard abbreviations used: Cx43, connexin 43; DTR, diphtheria toxin receptor; DTx, diphtheria toxin; fBV, blood volume fraction; IS, implantation site; MHCII, MHC class II; P4, progesterone; PS, permeability surface area product; sFlt1, soluble Flt1; uDC, uterine DC; uNK, uterine NK cell.

Conflict of interest: The authors have declared that no conflict of interest exists.

Citation for this article: *J. Clin. Invest.* doi:10.1172/JCI36682.

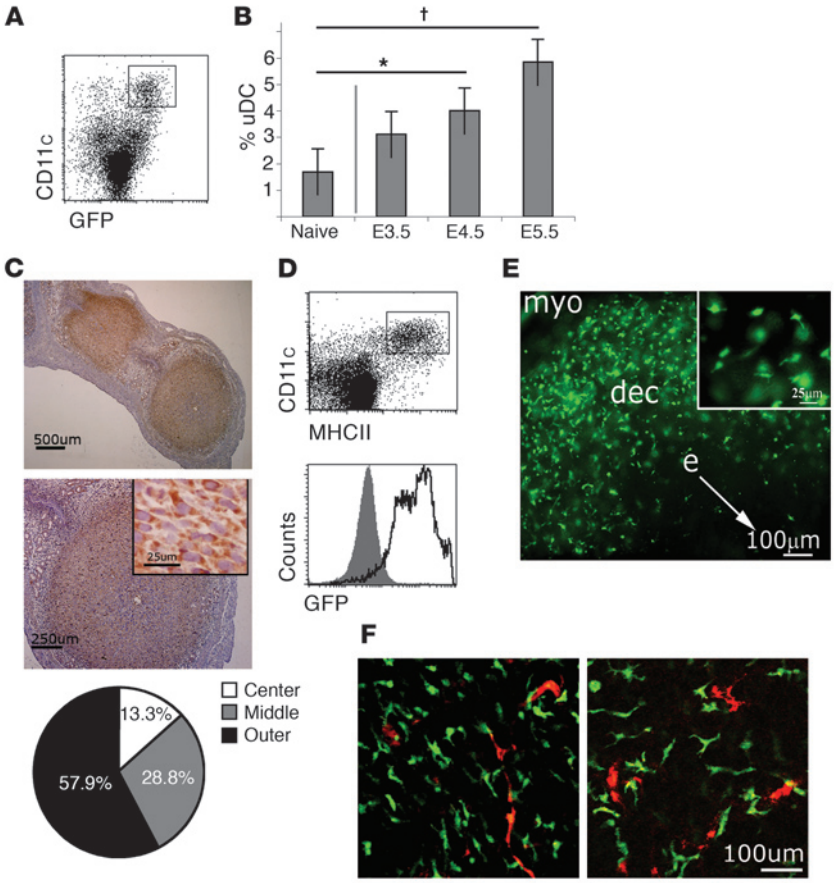

Figure 1
Anatomic localization of uDCs accumulating during embryo implantation. (**A**) Flow cytometry analysis of E5.5 IS of a CD11c:DTR transgenic mouse. Note the CD11c^{hi} uDC population, which expresses the DTR/GFP transgene. (**B**) Mean uDC percentages prior to and during implantation. uDCs of CD11c:DTR transgenic mice were defined as in **A**. Naive uteri (n = 3), E3.5 uteri (n = 2), E4.5 uteri (n = 5; *P = 0.007), and E5.5 uteri (n = 5; †P = 0.009). (**C**) Anti-GFP immunostaining (brown) of E5.5 uDCs of CD11c:DTR transgenic mouse (2 upper panels). Pie chart (lower panel) demonstrating quantifications of uDC distribution in the decidua. IS center, radius of 250 μm; middle rim, radius of 375 μm; outer rim, radius of 250 μm. The percentage of cells in the center is significantly smaller as compared with that in the middle (P = 0.009) and outer (P = 0.04) rims. (**D**) FACS analysis of *Cx$_3$cr1$^{gfp/+}$* IS. uDCs are gated as CD11c^{hi}MHCII^{hi} cells. Histograms represent uDCs (black line) and non-uDCs (filled). (**E**) Fluorescence microscopy analysis of ex vivo decidual tissue demonstrating localization of GFP$^+$ uDCs (green). (**F**) Two-photon microscopy demonstrating localization and morphology of uDCs (green) and blood vessels (red) in E5.5 IS. myo, myometrium; dec, decidua; e, embryo.

Earlier studies have described the presence of DCs in the nonpregnant endometrium in both humans and rodents (11, 12, 16). Furthermore, DCs accumulate in the pregnant uterus prior to implantation and remain through most of the pregnancy in the decidua (11, 12, 16). However, only limited information is available about these uterine DCs (uDCs) with respect to their phenotype, exact anatomical localization, and — most importantly — function throughout gestation and specifically during embryo implantation.

Here we investigated the function of uDCs during embryo implantation using an experimental system that allows the ablation of uDCs in the intact animal (17). Depletion of uDCs resulted in a severe impairment of the implantation process and led to embryo resorptions. Depletion of uDCs caused resorptions in syngeneic and T cell–deficient pregnancies, and deciduae failed to adequately form even in the absence of embryos after artificial decidualization. Depletion of uDCs was associated with impaired decidual proliferation and differentiation, as well as perturbed angiogenesis characterized by reduced vascular expansion and maturation. Collectively, our data suggest that uDCs govern uterine receptivity independent of their anticipated role as APCs by regulating tissue remodeling and angiogenesis through provision of critical factors, such as sFlt1 and TGF-β1, that synergistically promote coordinated blood vessel maturation.

Results

uDCs accumulate in the IS and undergo characteristic changes during pregnancy progression. DCs have been reported to accumulate in the maternal tissue surrounding the implanting embryo (12, 16). However, the role of these cells for implantation and pregnancy maintenance remains poorly understood. Our first objective was to characterize the distribution of uDCs during pregnancy. For this, we took advantage of transgenic mice that harbor uDCs that are labeled by expression of a GFP reporter (CD11c:diphtheria toxin receptor [CD11c:DTR] and *Cx$_3$cr1^{gfp}* mice; refs. 17, 18) (Figure 1, A and D). Flow cytometry analysis of uDCs prior to (naive) and during implantation (E3.5 until E5.5) demonstrated an increase in the number of uDCs with pregnancy progression (Figure 1, A and B). Furthermore, GFP immunostaining revealed that uDCs were concentrated at the IS and were particularly abundant in the outer rim of the decidua (Figure 1C). In order to visualize uDCs in live tissue, we used the *Cx$_3$cr1^{gfp}* model (18), in which uterine CD11c^{hi}MHCII^{hi} DCs that express CX$_3$CR1 are GFP labeled (Figure 1D). Analysis of uDC localization using this model confirmed the concentration of the uDCs in the decidual rim (Figure 1E). Two-photon microscopic analysis of E5.5 ISs revealed the distinct dendritic morphology of uDCs, localized at the IS, that were in close proximity to blood vessels (Figure 1F, Supplemental Video 1, and Supplemental Figure 1A; supplemental material available online with this article; doi:10.1172/JCI36682DS1). Next, we characterized the phenotype of uDCs by flow cytometry analysis. At E5.5, 5%–6% CD11c^{hi} DCs were observed at the IS (Figure 2A). This population displayed relatively low expression of the classical macrophage marker F4/80 (19), exhibited high MHCII levels, and expressed low levels of the DC maturation molecules CD86 and CD40. Furthermore, E5.5 uDCs expressed the mucosal DC marker CD103 (20). To probe for the existence of uDC subpopulations, we

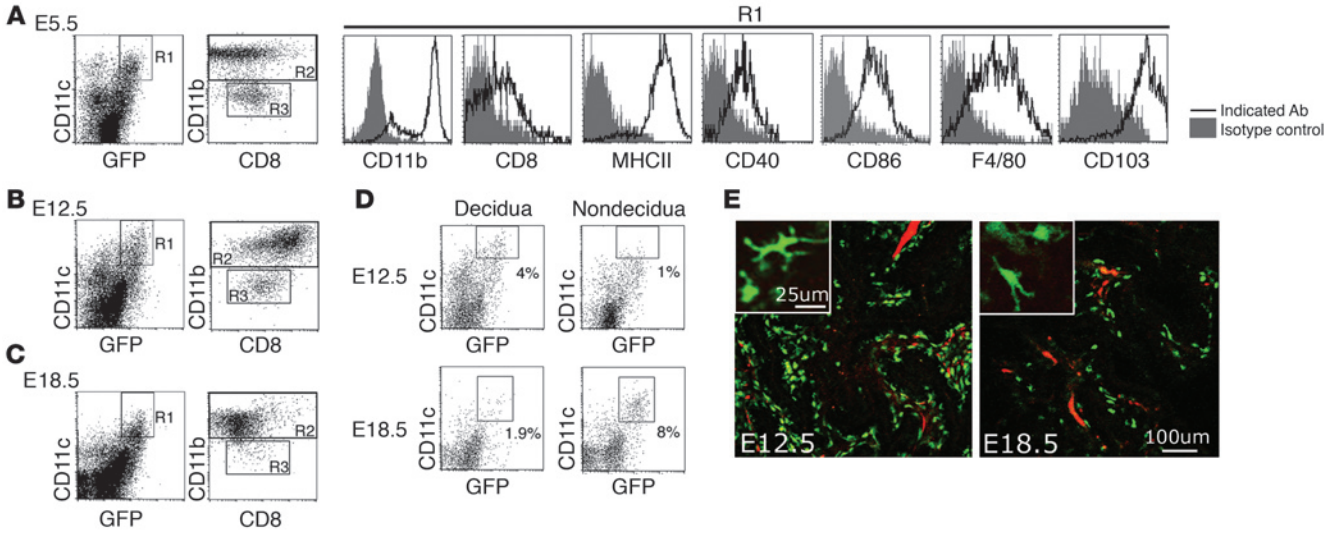

Figure 2

Phenotypic and localization differences of uDCs during pregnancy progression. (**A**) Flow cytometry profile of uDCs isolated from untreated mice (CD11c:DTR transgenic, C57BL/6). uDCs are gated as $CD11c^{hi}GFP^{+}$ cells (R1) and stained for CD11b and CD8α. Cells gated in the R2 and R3 regions are $CD11b^{hi}$ and $CD11b^{lo}$ uDCs. Histograms represent $CD11c^{hi}GFP^{+}$ cells from ISs at E5.5 that are stained with the indicated antibodies (black line) and respective isotype controls (filled) (R1, 4.5%; R2, 77%; R3, 23%) (E5.5; $n = 3$). (**B**) Flow cytometric profile of cells from E12.5 decidua (R1, 5.5%; R2, 85%; R3, 15%) (E12.5; $n = 3$). (**C**) Flow cytometric profile of cells from E18.5 myometrium (R1, 4%; R2, 94%; R3, 6%) (E18.5; $n = 3$). (**D**) Flow cytometry data for decidual and nondecidual tissues from E12.5 and E18.5 ISs. (**E**) Two-photon microscopic analysis of E12.5 and E18.5 endometrium of $Cx_3cr1^{gfp/+}$ mice, demonstrating the morphology of uDCs (green; cells with dendrites) and their localization in close proximity to blood vessels (red).

analyzed the cells for CD11b and CD8α expression, i.e., molecules that characterize the 2 main subsets of conventional splenic DCs (21). At E5.5, uDCs could be subdivided into $CD11b^{hi}CD8\alpha^{lo}$ and $CD11b^{lo}CD8\alpha^{lo}$ cells. The above-described uDC characteristics were unique to the early pregnancy, as analysis of uDCs at mid- (E12.5) and late (E18.5) pregnancy revealed distinct phenotypes. Thus, on E12.5, $CD11c^{hi}$ uDCs expressed more F4/80 and were activated, as indicated by their upregulation of MHCII and expression of CD86 and CD40 (Table 1). While we still observed 2 main subpopulations, the $CD11b^{hi}$ DCs expressed higher levels of CD8α (Figure 2B). uDCs at E18.5 were all of the $CD11b^{hi}CD8\alpha^{lo}$ phenotype (Figure 2C), expressed high levels of F4/80, and exhibited an immature phenotype ($CD86^{int}CD40^{lo}$) (Table 1). Interestingly, the different pregnancy stages also showed a distinct anatomic distribution of uDCs in the uterus. While on E5.5 and E12.5 of pregnancy, uDCs were found mainly in the decidualized tissue at the embryo IS (Figure 1A) and decidua basalis (Figure 2D), respectively, uDCs on E18.5 were mostly localized to the nondecidualized uterine tissue (Figure 2D). Moreover, two-photon microscopy revealed that uDCs on day E12.5 (Figure 2E, Supplemental Video 2, and Supplemental Figure 1B) and E18.5 (Figure 2E, Supplemental Video 3, and Supplemental Figure 1C) were even more closely associated with blood vessels as compared with E5.5 uDCs. The distinct phenotypes and localization of uDCs at the IS suggested that these cells might have distinct roles during different pregnancy stages and specifically during embryo implantation, a decisive phase of pregnancy.

Conditional ablation of uDCs during the implantation window results in embryo resorption. To investigate the role of uDCs during embryo implantation, we took advantage of the CD11c:DTR mouse model, which allows the conditional ablation of $CD11c^{hi}$ DCs by diphtheria toxin (DTx) administration (17). We originally chose to work with a semiallogeneic model, as DCs were hypothesized to have a tolerogenic role in pregnancy. Semiallogeneic pregnant mice were treated by i.p. injection of DTx on E.3.5, i.e., just before implantation, and were analyzed on E4.5 and E5.5 (Figure 3). DTx injection led to the rapid depletion of $CD11c^{hi}$ DCs within 8 hours and lasted for at least 2 days (17), thus covering the implantation window (which starts on E4 and concludes on E5.5). For control, we injected either E3.5 CD11c:DTR mice with PBS or E3.5 WT mice with DTx (Supplemental Figure 2). It is noteworthy that uterine macrophages remained unaffected by the DTx administration (Supplemental Figure 3, A and B). uNKs included both DTR/GFP^{+} and DTR/GFP^{-} subpopulations (Supplemental Figure 3D); however, under the conditions used (1 ng/g body weight DTx), uNKs were not ablated (Supplemental Figure 2C).

Uterine sections of E4.5 control mice bearing uDCs (Figure 3A) were characterized by the presence of developing implantation

Table 1

Analysis of uDC phenotypes during different pregnancy stages

	E5.5	E12.5	E18.5
CD8	43 ± 10	495 ± 133	69 ± 28
MHCII	1,353 ± 359	2,022 ± 353	1,229 ± 732
CD86	60 ± 7	620 ± 39	396 ± 48
CD40	26 ± 5	168 ± 31	18 ± 16
F4/80	310 ± 24	3,078 ± 678	4,135 ± 693
CD103	2,093 ± 195	4,834 ± 253	1,771 ± 756

Values are the MFI of the indicated markers (stained minus isotype control).

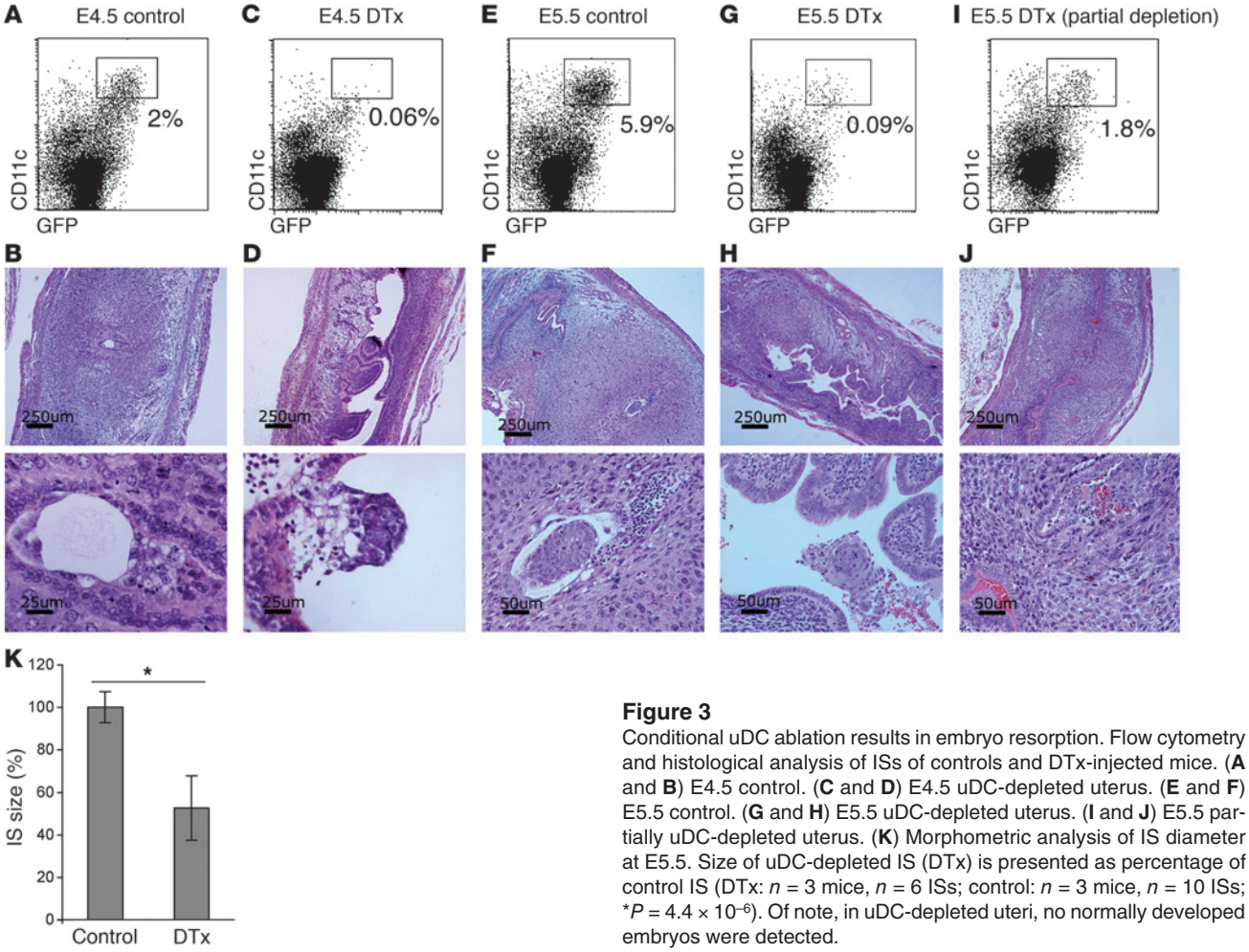

Figure 3

Conditional uDC ablation results in embryo resorption. Flow cytometry and histological analysis of ISs of controls and DTx-injected mice. (**A** and **B**) E4.5 control. (**C** and **D**) E4.5 uDC-depleted uterus. (**E** and **F**) E5.5 control. (**G** and **H**) E5.5 uDC-depleted uterus. (**I** and **J**) E5.5 partially uDC-depleted uterus. (**K**) Morphometric analysis of IS diameter at E5.5. Size of uDC-depleted IS (DTx) is presented as percentage of control IS (DTx: $n = 3$ mice, $n = 6$ ISs; control: $n = 3$ mice, $n = 10$ ISs; $^*P = 4.4 \times 10^{-6}$). Of note, in uDC-depleted uteri, no normally developed embryos were detected.

chambers. We could observe embryos attached to the uterine wall initiating the process of invasion toward the uterine stroma, which showed characteristics of proliferation and differentiation into a decidua (Figure 3B). In contrast, DTx-treated CD11c:DTR transgenic mice lacking uDCs (Figure 3C) harbored nonreceptive uteri, in which the implantation chamber failed to form adequately. The uterine lumen was open, the decidualization process was severely impaired, and embryos neither attached to nor invaded the uterine epithelium (Figure 3D). On E5.5, control mice exhibited significantly expanded deciduae, and the embryo developed into the egg cylinder stage (Figure 3, E and F). In contrast, the uDC-depleted uteri exhibited reduced decidualization, and only rarely were embryos found in the uterus, mostly detached from the uterine lumen and undergoing resorption (Figure 3, G and H).

In order to study the phenotype induced by uDC depletion in more detail, we titrated the DTx dose to achieve a partial depletion of uDCs (50%–70%; Figure 3I). Thus, some decidual tissue remained, and investigation of the mechanism underlying the embryo resorption was facilitated. Deciduae of mice that were subjected to this protocol were significantly reduced in size as compared with those of controls, and the respective embryos had undergone resorption (Figure 3, J and K). This indicated a linear correlation between the number of uDCs at the IS and decidua development. Compilation of the results from independent experiments showed that while control mice displayed normal implanted embryos, two-thirds of the DTx-treated CD11c:DTR mice had resorptions or completely lacked ISs, one-third had smaller and nondeveloped ISs, while none had normal ISs (Table 2).

To exclude the possibility that the systemic DC ablation had an indirect effect on the pregnancy, we performed a local uDC depletion. At E3.5, right uterine horns of mated females were injected with either DTx or PBS (control). Two days later (E5.5), the lower part of each horn was retrieved for histological examination, while the upper part was taken for flow cytometry (Figure 4J). FACS analysis confirmed a reduction in uDCs in the DTx-injected uterine horn (Figure 4G) but not in the contralateral control horn (Figure 4E). Histological sections revealed that the injected horn exhibited significantly smaller and malformed IS (Figure 4I), with retarded decidualization, and no embryos could be detected (Figure 4H). The contralateral uterine horn of the same mouse (Figure 4F), as well as the PBS-injected and noninjected horns of control mice that retained uDCs (Figure 4, A and C), exhibited normal IS with developed deciduae and embryos (Figure 4, B and D). Furthermore, we tested the effect of uDC depletion after successful implantation, i.e., on E5.5. Notably, uDCs were also readily depleted in this time point; however, there was no effect on the embryo fate or decidua development (Supplemental Figure 4). This result suggests a specific critical role for uDCs during the time window of

Table 2
Analysis of the effect of uDC depletion on embryo ISs

E5.5	CD11c:DTR + DTx	Control[A] (CD11c:DTR + PBS/WT + DTx)
No. mice with resorptions/no IS	13 (68%)	1 (5%) [1/0]
No. mice with impaired IS	6 (32%)	0 [0/0]
No. mice with normal IS	0	18 (95%) [12/6]
No. total mice	19	19 [13/6]

[A]Note that controls were composed of PBS-treated CD11c:DTR transgenic mice and DTx-treated WT mice, with number indicated in the square brackets.

embryo implantation and excludes nonspecific effects that the DTx administration or apoptosis of uDCs may have. Collectively, these results suggest that uDCs have a specific and direct role in decidual development and embryo implantation.

Embryo resorption does not result from breakage of immunological tolerance or adaptive immunity. It is widely assumed that DCs in the uterus are required to establish tolerance toward the semiallograft fetus (22, 23). To test this possibility, we compared the effect of uDC depletion we had obtained in the allogeneic system to a syngeneic pregnancy model. Interestingly, analysis of uDC-depleted uteri on E5.5 (Figure 5A) revealed similar phenotypes in the allogeneic and syngeneic pregnancy models. In both cases, morphometric analysis showed a significant reduction in IS sizes in uDC-depleted as compared with control uteri (Figure 5B). These results argue against a role of uDCs in tolerance induction during the implantation period. This notion is further supported by results from additional experiments involving pregnant females that lack T and B cells (CD11c:DTR *Rag*$^{-/-}$). Also in this setting, uDC depletion resulted in embryo resorption and a significant reduction in the size of the IS (Figure 5, C and D).

Impaired decidualization is induced by uDC depletion even in the absence of embryo. To establish whether the implantation defect caused by uDC depletion depends on the embryo or whether uDCs have a specific role in the decidua formation, we induced artificial decidualization in the absence of embryos (24). Thus, C57BL/6 CD11c:DTR females were mated with vasectomized BALB/c males, and the uteri of plug-positive females were sutured on E3.5 to induce decidualization. Animals were then administered either PBS or DTx. When analyzed on E5.5, uDC-depleted uteri exhibited malformed deciduae as compared with the well-developed artificial

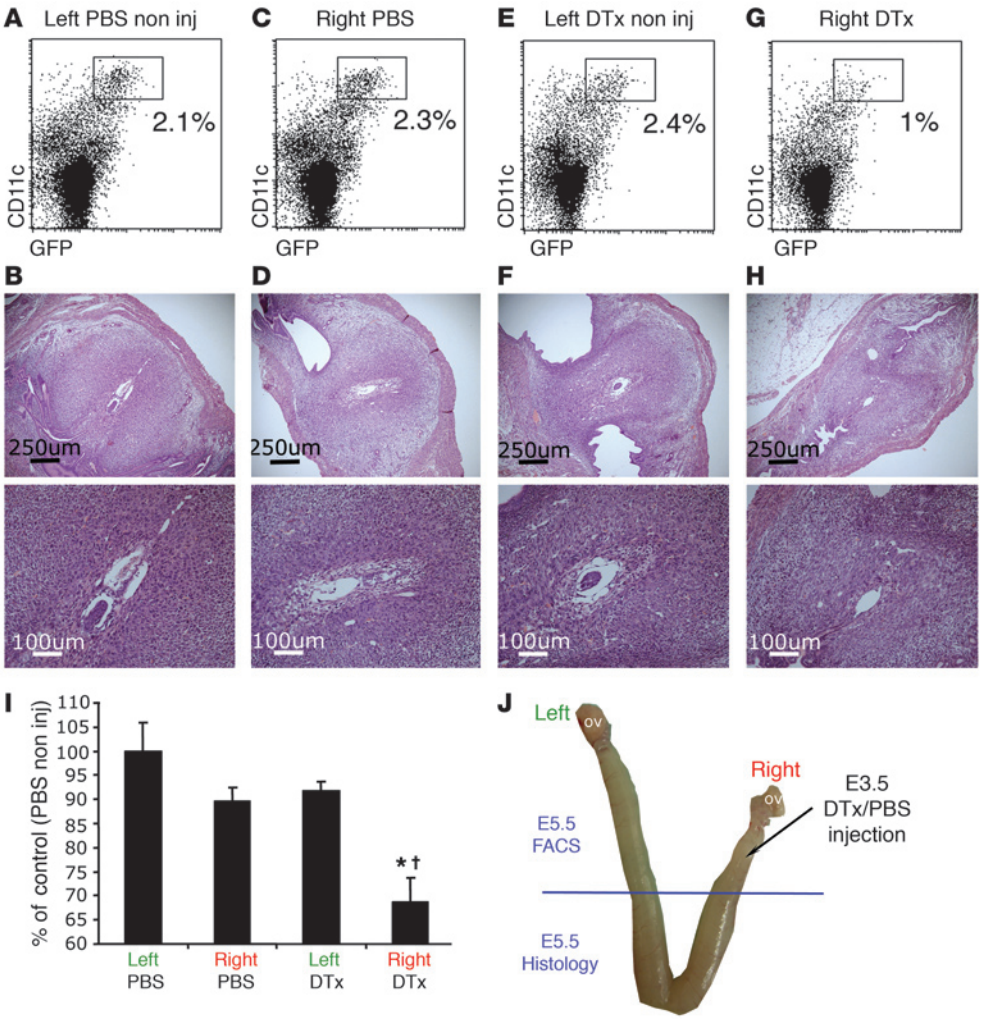

Figure 4
Local uDC depletion results in embryo resorption. On E5.5, all mice were sacrificed, and the lower parts of each horn were retrieved for histology, while the upper parts were taken for flow cytometry analysis. (**A** and **B**) Left noninjected uterine horn versus (**C** and **D**) right uterine horn, locally injected with PBS on E3.5 as a control. (**E** and **F**) Left noninjected uterine horn (non inj) versus (**G** and **H**) right uterine horn, locally injected with DTx on E3.5. (**I**) Morphometric analysis of IS diameter at E5.5. Size of uDC-depleted IS (DTx) is presented as percentage of control (PBS-noninjected) IS (DTx: $n = 2$, 2 injected IS, 2 noninjected IS; PBS: $n = 2$, 3 injected IS, 4 noninjected IS; $^*P = 0.03$, DTx right versus PBS right). Note that size of locally DTx-treated IS is significantly reduced compared with that of all other ISs ($^\dagger P < 0.04$ versus DTx left and PBS right and left). uDCs are identified as CD11c^{hi}GFP$^+$, and their percentages are indicated. (**J**) Experimental scheme. Uterine photograph (of a nonpregnant mouse) is only for illustration. OV, ovary.

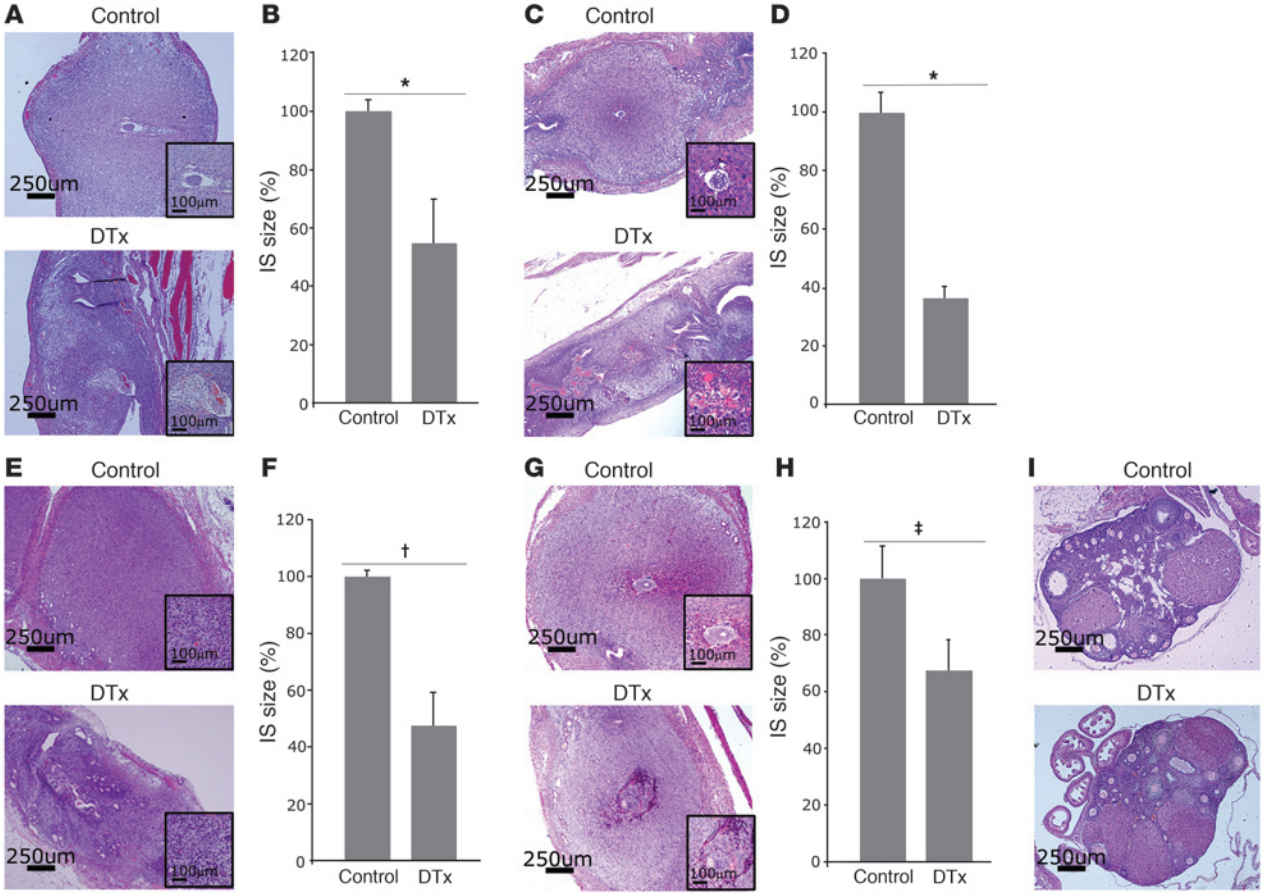

Figure 5

Decidualization failure is independent of immunity and occurs in absence of embryo. Representative histological sections of E5.5 uteri or ovaries and morphometric analysis. (**A** and **B**) Syngeneic model: CD11c:DTR transgenic females mated with C57BL/6 males (DTx: $n = 3$ mice, $n = 5$ ISs; control: $n = 2$ mice, $n = 3$ ISs; $^*P = 0.001$). (**C** and **D**) Lymphocyte-deficient model: *Rag2*$^{-/-}$ CD11c:DTR transgenic females mated with BALB/c males (DTx: $n = 2$ mice, $n = 8$ ISs; control: $n = 3$ mice, $n = 12$ ISs; $^*P = 0.001$). (**E** and **F**) Artificial decidualization: Females were mated with vasectomized BALB/c males and their uteri sutured on E3.5 (DTx: $n = 4$ mice, $n = 6$ artificial ISs; control: $n = 2$ mice, $n = 4$ artificial ISs; $^\dagger P = 0.00001$). (**G** and **H**) P4 administration in the allogeneic model. Pregnant females were injected s.c. with P4 on E3.5 and E4.5 (DTx: $n = 3$ mice, $n = 9$ ISs; control: $n = 3$ mice, $n = 13$ ISs; $^\ddagger P = 0.02$). (**I**) Ovaries of control versus DTx-injected females. Note that experimental groups were injected with 1 ng/g body weight DTx, resulting in partial ablation of uDCs.

control deciduae (Figure 5E). Morphometric analysis showed significant impairment in the development of the deciduae in uDC-depleted uteri (Figure 5F). These results suggest that the effect of uDCs on the development of the decidua is embryo independent, further emphasizing the irrelevance of embryo allogeneity in the process. Importantly, these results directly link uDCs to the decidualization process and suggest that the embryo resorption is caused by impaired uterine receptivity.

Progesterone does not rescue the implantation disorder caused by DC-depletion. Corpus luteum–derived progesterone (P4) plays a crucial role in embryo implantation and subsequent pregnancy development by maintaining decidual viability and inhibiting myometrial contractility (25). To test whether the implantation failure observed in response to uDC depletion is a result of corpus luteum insufficiency, we tried to rescue the pregnancies by P4 administration on E3.5 and E4.5. P4 treatment did not prevent embryo resorption induced by uDC depletion (Figure 5, G and H). Furthermore, evaluation of the ovaries demonstrated that the uDC-depleted females exhibited corpora lutea with normal morphology as compared with control mice (Figure 5I). Therefore, we conclude that the implantation failure in the absence of uDCs is not due to lack of P4 production.

Impaired proliferation, decidual differentiation, and vascular expansion in uDC-depleted ISs. Our results suggest that decidualization depends on uDCs. To elucidate the underlying mechanism, we decided to analyze two hallmarks of decidua formation: cell proliferation and differentiation. The proliferation status of decidual cells was investigated on partially uDC-depleted uteri, which still retain some decidual cells. Immunostaining for phospho–histone H3 (Figure 6, A and B) as a proliferation marker (26) revealed extensive cell proliferation in the control mice. In contrast, uDC-depleted deciduae were largely devoid of proliferation. To study the impact of the uDC depletion on decidual differentiation, we investigated the induction of connexin 43 (Cx43), a gap junction protein expressed at the onset of embryo implantation, which is an established decidual differentiation marker (27). Immunohistochemical

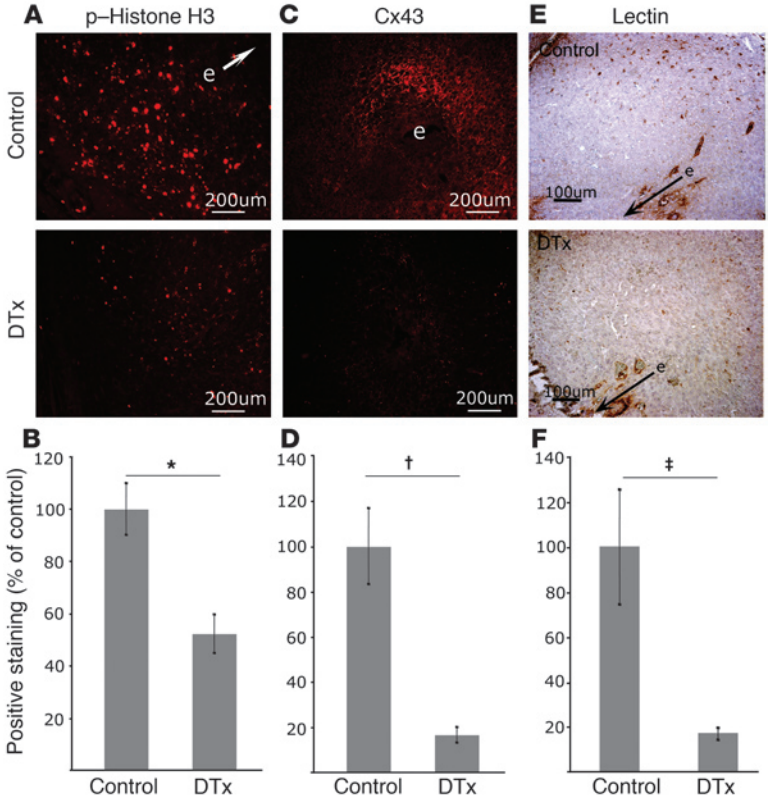

Figure 6
Proliferation, decidual differentiation, and vascular expansion characterizing decidualization are impaired in uDC-depleted ISs. (**A**) Immunohistochemistry for phospho–histone H3 indicated upon reduced cell proliferation in the decidua of uDC-depleted ISs. (**B**) Quantification analysis of phospho–histone H3 staining in uDC-depleted ISs, shown as percentage of control (DTx: $n = 2$ mice, $n = 3$ ISs; control: $n = 2$ mice, $n = 3$ ISs; $^{*}P = 0.022$). (**C**) Cx43 staining indicative of reduced cell proliferation in the decidua of uDC-depleted ISs. (**D**) Quantification of Cx43 staining in uDC-depleted IS, shown as percentage of control (DTx: $n = 2$ mice, $n = 3$ ISs; control: $n = 2$ mice, $n = 3$ ISs; $^{\dagger}P = 6.5 \times 10^{-5}$). (**E**) Immunostaining for endothelial cells using lectin (brown) of control versus uDC-depleted (DTx) E5.5 ISs. Note the reduced vessel density of uDC-depleted ISs versus control. (**F**) Quantification of lectin staining in uDC-depleted ISs, shown as percentage of control (DTx: $n = 2$ mice, $n = 3$ ISs; control: $n = 2$ mice, $n = 3$ ISs; $^{\ddagger}P = 0.044$). e, direction of embryo location. In uDC-depleted uteri, embryo location was not indicated, since the embryo is resorbed in these specific histological preparations.

analysis for Cx43 in the control revealed prominent expression in the primary decidual zone (Figure 6, C and D). In contrast, Cx43 expression was significantly reduced in the uDC-depleted uteri, indicative of impaired decidual differentiation. Finally, we looked at the impact of uDC absence on decidual vascular expansion, a major prerequisite for adequate implantation. Immunostaining for endothelial cells using lectin (Figure 6, E and F) revealed reduced capillary density of uDC-depleted ISs versus control, implying an angiogenic disorder associated with uDC absence. Overall, uDC depletion caused severe impairment of all major characteristics of decidualization: stromal cell proliferation and differentiation, as well as vascular expansion were severely damaged, thus preventing the formation of an adequate decidual tissue.

Functional analysis of decidual vascular function revealed impaired angiogenesis in uDC-depleted ISs. The reduced capillary density exhibited after uDC depletion implied a major perturbation in decidual angiogenesis — a dynamic, precisely timed process that critically affects uterine receptivity. Decidual angiogenesis is characterized by increased vascular permeability on E4.5 followed by a rise in blood volume on E5.5 and can be investigated noninvasively by dynamic macromolecular-contrast enhanced MRI (28). Interestingly, we were unable to detect E4.5 uDC-depleted ISs by MRI, indicating the presence of low angiogenic activity below quantifiable levels compared with controls (Supplemental Figure 5A). On E5.5, uDC-depleted ISs were significantly smaller and showed reduced contrast enhancement relative to controls, as detected by MRI (Figure 7, A, B, and E, and Supplemental Figure 5B). The blood volume fraction (fBV) calculated using the MRI data was significantly lower in uDC-depleted ISs (Figure 7C). However, the permeability surface area product (PS) of uDC-depleted ISs was similar to that of the control (Figure 7D). This suggested that the transcapillary leak of plasma proteins was higher in E5.5 uDC-depleted ISs, i.e., that blood vessels in the uDC-depleted deciduae were more permeable than those of the controls. The MRI results were corroborated by fluorescence analysis. E5.5 decidual blood vessels were undetectable in uDC-depleted ISs, 3 minutes after MR contrast material injection, and at 15 minutes, only a minor part of the contrast material had extravasated in uDC-depleted sites as compared with control (Figure 7F). Quantitative analysis (Figure 7G) revealed significantly reduced fluorescence of the decidual part in uDC-depleted ISs, indicating reduced vessel density and similar permeability. E4.5 ISs exhibited similar, although less pronounced trends than E5.5 ISs, as the decidua was less extended (Supplemental Figure 5, C and D). Overall, dynamic contrast-enhanced MRI–assisted studies revealed reduced blood volume and enhanced capillary leak, suggesting a role for uDCs not only in decidual vascular expansion but also in subsequent vascular maturation and attenuation of vascular permeability. This finding is consistent with the reduced density of vascular smooth muscle cells, immunostained using anti–α-SMA (Figure 7, H and I), of control versus uDC-depleted E5.5 ISs. The absence of mature blood vessels (with pericyte or vascular smooth muscle cell coating) from the rim of the uDC-depleted IS may account for the elevated transcapillary leak of plasma proteins in uDC-depleted deciduae.

uDCs directly control decidual angiogenesis by regulating vascular maturation. The results of the MRI analysis and the α-SMA of uDC-depleted ISs revealed a strikingly enhanced capillary leak and the presence of immature blood vessels. In search of a molecular mechanism to explain the requirement of uDCs in the implantation process, we decided to focus on a potential link of uDCs to

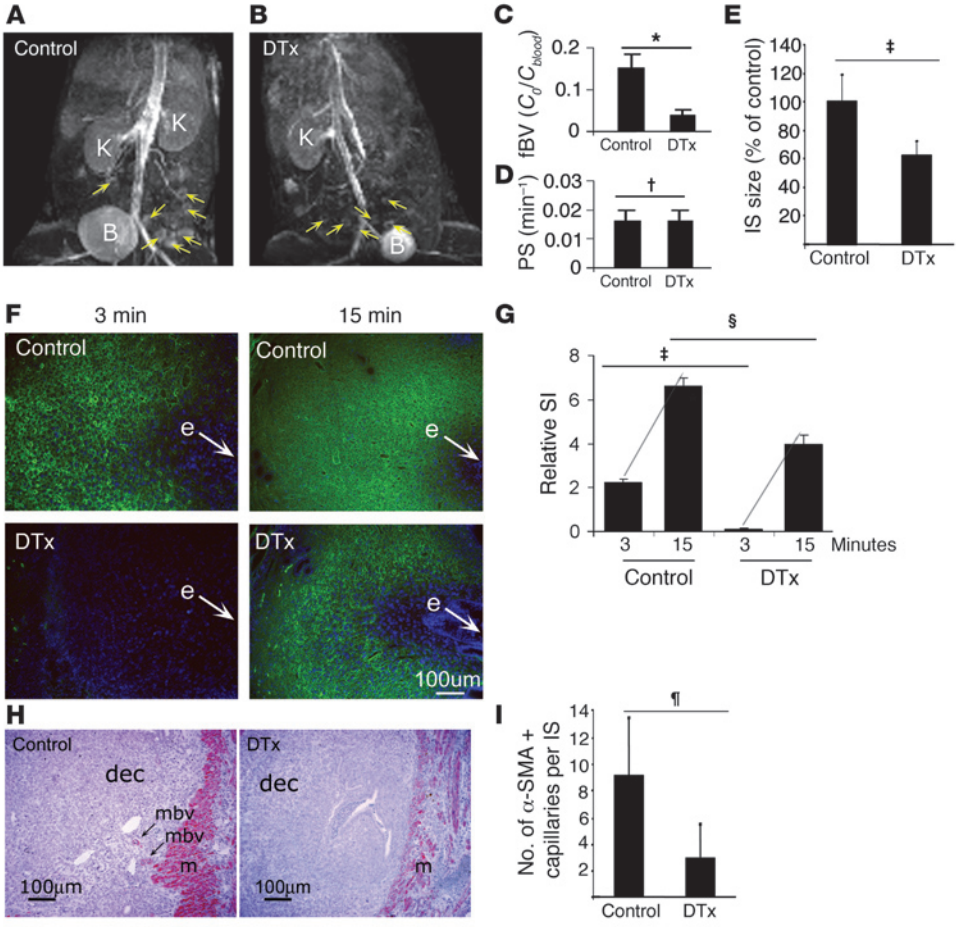

Figure 7

Functional analysis of decidual vascular function reveals impaired angiogenesis in uDC-depleted ISs. (**A** and **B**) 3D gradient-echo MRI maximal intensity projections, 24 minutes after biotin-BSA-GdDTPA injection. (**C**) fBV and (**D**) PS (control: $n = 3$ mice, 10 ISs; DTx: $n = 2$ mice, 6 ISs; $^*P = 0.03$, $^\dagger P = 0.89$). (**E**) Quantitative analysis of IS size measured by MRI. Size of uDC-depleted ISs (DTx) is presented as percentage of control ISs (control: 3 mice, $n = 10$ ISs; DTx: 2 mice, $n = 6$ ISs: $^\ddagger P = 0.0011$). (**F** and **G**) ISs were retrieved 3 and 15 minutes after biotin-BSA-GdDTPA injection and stained with avidin-FITC ($n = 2$ mice, $n = 3$ ISs per time point; $^\ddagger P = 1.6 \times 10^{-5}$, $^\S P = 0.002$). Gray trend lines indicate permeability (signal intensity [SI] at 15 minutes minus SI at 3 minutes: control, 4.4; DTx, 3.8). Yellow arrows, IS; white arrows, embryo location; B, bladder; K, kidney; e, embryo; ni, nonimplanted uterine site. (**H**) Immunostaining for smooth muscle cells using anti–α-SMA (red) of control versus uDC-depleted (DTx) E5.5 ISs. Note the absence of mature blood vessels (with α-SMA coating) from the edges of the uDC-depleted IS. Myometrium stained positive for α-SMA. m, myometrium; mbv, maternal blood vessel. (**I**) Quantitation of α-SMA–positive capillary number per IS showing uDC-depleted IS compared with control (DTx: $n = 2$ mice, $n = 4$ ISs; control: $n = 2$ mice, $n = 9$ ISs; $^\P P = 0.026$).

angiogenesis and vascular maturation. Vascular plasticity during angiogenesis is driven by VEGF, which elevates vascular permeability. The activity of VEGF is in turn under the control of a physiological "VEGF trap" in the form of a secreted VEGF receptor 1 (Flt1) (29). Interestingly, quantitative RT-PCR analysis of FACS-sorted uDCs and fractionated decidual tissue revealed that in the IS, this soluble Flt1 (sFlt1) is expressed by uDCs but not by decidual NK cells (Figure 8, A and B). This result suggests that one role of uDCs in the decidua is to fine-tune angiogenesis and vascular permeability by secretion of sFlt1. This potential scenario is further strengthened by the immunohistochemical analysis of ISs: here we found a significantly decreased immunoreactivity to sFlt1-specific antibody in uDC-depleted deciduae (Figure 8, C and D) specifically in the decidual rim, where uDCs accumulate (Figure 8E). Our expression analysis of decidual cells further revealed that uDCs express TGF-β1 (Figure 8F), a cytokine with pleiotropic functions that can directly affect vascular maturation (30) and promotes endothelial cell survival. As opposed to expression of sFlt1, TGF-β1 expression was shared with uNKs. However, interestingly, the RT-PCR analysis of uDC-depleted ISs revealed a global reduction in TGF-β1 expression (Figure 8, G and H). Taken together, our results suggest that uDCs are directly involved in the fine-tuning of angiogenesis in the decidua through provision of two critical factors, sFlt1 and TGF-β1, that act synergistically to promote coordinated vascular expansion and maturation.

Discussion

Here we performed a functional characterization of uDCs with respect to their involvement in embryo implantation using an in vivo cell ablation strategy. Depletion of uDCs resulted in severe impairment of the implantation process and led to embryo resorptions. Rather than being involved in tolerance establishment, uDCs seem to regulate maternal receptivity through direct involvement in decidual tissue remodeling and specifically angiogenesis. Flow cytometric, histological, and in vivo characterization of uDCs during implantation and later pregnancy stages revealed distinct phenotypes and microanatomical localizations, suggesting discrete functions with pregnancy progression. Indeed, depletion of uDCs immediately after the conclusion of the implantation process did not lead to embryo loss. At the time of implantation (E5.5), uDCs exhibited an immature phenotype, characteristics of mucosal DCs, and could be subdivided into two subpopulations according to CD11b and CD8α expression. Moreover, uDCs at E5.5 were found in close proximity to blood vessels. To study the functional role of uDCs in implantation, we used a conditional ablation strategy to deplete the cells before the embryo makes its first contact with the uterus and throughout the entire implantation window (E4 until E5.5). uDC ablation resulted in embryo resorption. The remainder of our study was devoted to the investigation of the physiological and molecu-

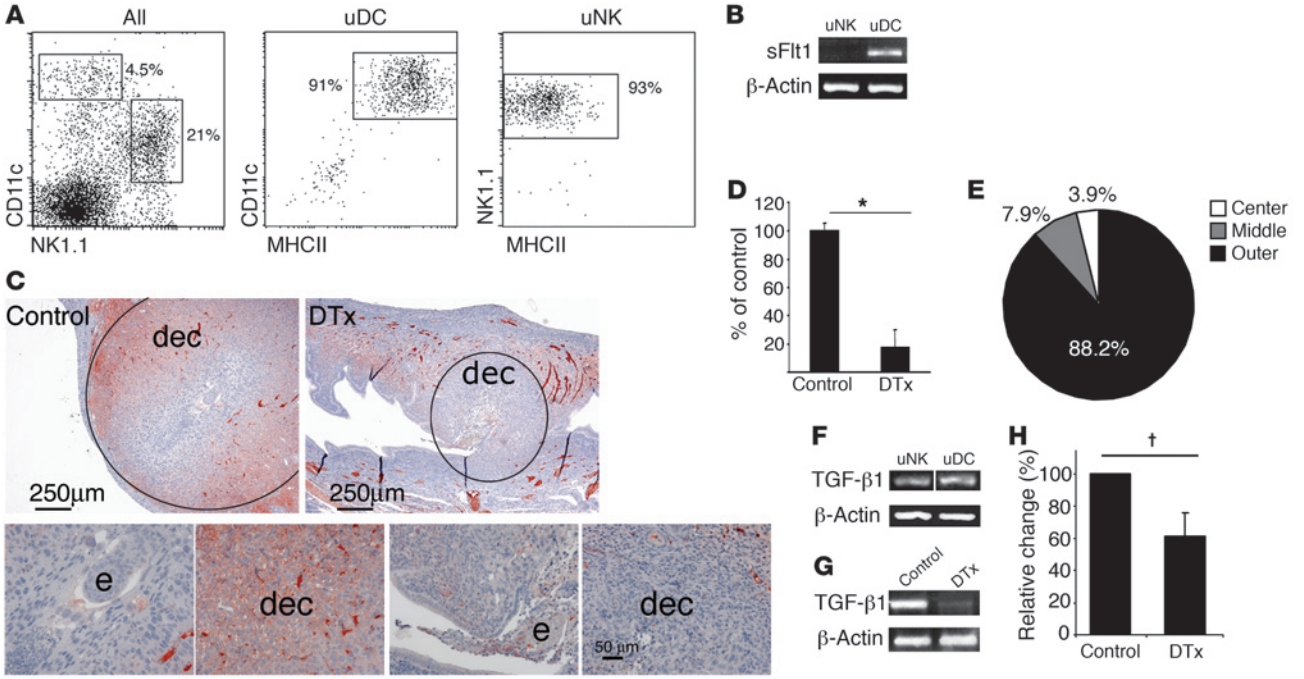

Figure 8

Evidence for a direct role for uDCs in decidual angiogenesis by regulating vascular maturation. (**A**) Flow cytometry analysis of decidual cells (All) sorted for uNKs and for uDCs. (**B**) Semiquantitative RT-PCR for sFlt1 of the sorted cells in **A**. (**C**) Immunostaining for sFlt1 (brown) of control versus uDC-depleted (DTx) E5.5 ISs. Note that in the control ISs, sFlt1 staining is most abundant in the outer decidual rim, which is the localization of uDCs and also the localization of α-SMA–positive mature vessels (Figure 7H). In uDC-depleted deciduae, the sFlt1 staining is absent. Decidual tissue is circled. (**D**) Quantification of sFlt1 staining in uDC-depleted IS is shown as percentage of control (DTx: $n = 2$ mice, $n = 3$ ISs; control: $n = 2$ mice, $n = 3$ ISs; $^*P = 0.0035$). Data quantification was performed on the whole IS (not only the decidua) to avoid bias. (**E**) Quantifications of sFlt1 distribution in the decidua. Radius of IS center, 240 μm; middle rim, 350 μm; outer rim, 240 μm. Note that the percentage of cells in the outer rim is significantly higher than that in the middle ($P = 0.0012$) and center ($P = 0.0018$). (**F**) Semiquantitative RT-PCR for TGF-β1 of the sorted cells in **A**. The bands were run on the same gel at the same time but were not contiguous. (**G**) Semiquantitative RT-PCR for TGF-β1 of uDC-depleted and control IS and (**H**) quantitative analysis of 3 different experiments. $^\dagger P < 0.05$.

lar mechanisms that underlie this unique requirement of uDCs for embryo implantation.

The presence of immune cells at the IS has long been associated with the response of the maternal immune system to the semiallogeneic fetus (22, 23). However, presentation of fetal antigen was reported to begin only at mid-gestation, in association with the endovascular invasion of placental trophoblasts and the hematogenous release of placental debris (31). Accordingly, our results that focus on the implantation window suggest that uDCs are not required for tolerance establishment. Thus, uDC ablation also resulted in embryo resorption in syngeneic and T cell–deficient pregnancy models. Moreover, depletion of uDCs impaired artificial decidualization induced in pseudopregnant mice in the absence of an embryo.

The maintenance of pregnancy and specifically the decidualization process requires P4, a principal steroid hormone secreted by the corpus luteum (32). However, in our model, the embryo loss induced by uDC depletion could not be rescued by P4 administration and is, therefore, unrelated to corpus luteum insufficiency. Interestingly, we rather found that the uDC ablation directly affected three critical parameters of the decidualization process: proliferation, differentiation, and angiogenesis. Immunohistochemical analysis of uDC-depleted ISs for phospho–histone H3 and Cx43 revealed an impairment of proliferation and decidual differentiation. Along with reduced expression of lectin in the uDC-depleted IS, noninvasive functional analysis of angiogenesis by dynamic macromolecular contrast-enhanced MRI revealed significant perturbances within the 2 days of the implantation window in uDC-depleted ISs. Angiogenesis during normal embryo implantation is characterized by increased vascular permeability on E4.5, followed by a rise in blood volume on E5.5. By the end of the implantation process (E5.5) and along with the attenuation of vascular permeability, blood vessels undergo maturation (28). Upon uDC depletion, the formation of new blood vessels in the decidua was significantly reduced on E5.5, and vascular maturation was impaired, showing higher permeability per blood vessel, a characteristic of the initiation of the implantation process (E4.5). uDC ablation thus resulted in a delayed decidual angiogenic response. Given the limited time window in which the uterus is receptive toward the implanting embryo (33), impaired angiogenesis results in a failure of the embryo to implant into the uterine wall (34). In support of a suggested role for uDCs in decidual vascular development, uDCs are associated with blood vessels, as exhibited in the functional analysis using MRI and fluorescence microscopic data.

Physiological angiogenesis is a fine balance between pro- and antiangiogenic factors (34). Vascular plasticity during angiogenesis is driven by VEGF, which is a potent vascular permeability factor. In pregnant mice, VEGF expression is observed in the luminal

epithelium as early as day 1. VEGF is also expressed by stromal cells (35, 36), as well as uNKs and macrophages (7, 35). In light of the abundance of VEGF expression in the decidua, VEGF levels require local modulation to facilitate tissue remodeling and allow decidual transformation. One of the key molecules in the control of VEGF activity is a physiological VEGF trap in the form of a secreted VEGF receptor 1 (Flt1) (29) that locally sequesters the proangiogenic factor to execute its effect on vascular permeability. Interestingly, our expression analysis of fractionated decidual tissue revealed that in the IS, sFlt1 is expressed by uDCs but not by uNKs. Moreover, the critical importance of this uDC-derived sFlt1 in the local control of angiogenesis is highlighted by the fact that immunoreactivity to anti-sFlt1 antiserum in the outer decidual rim, i.e., the exact location of the bulk of uDCs, was significantly reduced in uDC-depleted ISs. Our data thus strongly suggested that a key role of uDCs in decidua formation is to fine-tune angiogenesis by specifically attenuating vascular permeability via secretion of sFlt1. In the absence of uDCs, sFlt1 is missing, vascular permeability is not attenuated, and subsequent vascular maturation at the boundaries of the IS do not occur.

Our expression analysis of decidual cells further revealed that uDCs express the cytokine TGF-β1. Moreover, although TGF-β1 expression was shared with uNKs, the analysis of uDC-depleted ISs revealed a general reduction in the expression level of this cytokine. Notably, our data do not exclude the possibility that TGF-β1 expression by uNKs could also be driven by uDC-uNK crosstalk. The reduction of TGF-β1 in uDC-depleted IS might have multiple consequences. First, as TGF-β1 can promote endothelial cell survival (37), TGF-β1 that is directly produced by uDCs could be critically required to locally quench a potential proapoptotic activity that has been reported for sFlt1 (as it sequesters VEGF, an endothelial cell survival factor) (38) and thus provide crucial protection for the uDC-associated endothelial cells. This may ensure that the VEGF trap sFlt1 expressed by uDCs will only act to sequester VEGF activity as a permeability factor but will be less effective in causing endothelial cell death in the presence of TGF-β1.

Second, TGF-β is known to directly affect vascular maturation through its effect on endothelial–smooth muscle cell interactions (30, 37). Vascular maturation at the IS mostly occurs at the edges of the IS, and the observed global reduction of TGF-β1 in uDC-depleted ISs could thus have a major effect on the ability of these blood vessels to mature. Finally, the absence of TGF-β1 was previously proposed to have a direct effect on the proliferation and decidualization of stromal cells (30). However, this might be secondary to the angiogenic disorder, since tissue growth and remodeling are critically dependent on proper vascular expansion.

Taken together, our results suggest that uDCs fine-tune angiogenesis in the decidua through provision of two critical factors, sFlt1 and TGF-β1, that act together to promote coordinated vascular expansion and maturation. In their absence, vascular permeability is increased, blood volume is reduced, and vessel maturation is attenuated, resulting in a fatal delay of the angiogenic reaction. This leads to faulty tissue remodeling, which causes the embryo loss. The specific localization of uDCs in the outer decidual rim and in proximity to blood vessels supports their role in attenuating permeability, promoting vascular survival and vessel maturation, which occur mainly at the edges of the IS. Of note, however, our data do not exclude more complex settings in which uDCs would provide multiple crucial factors to the decidualization and subsequent angiogenesis involving additional cell types.

In summary, we demonstrated a role for uDCs in successful embryo implantation, which is directly associated with adequate decidualization by coordinating the synchronization between uterine receptivity and embryo development. These results provide a new perspective on DC functions during pregnancy beyond their anticipated tolerogenic effect, suggesting a more active role in tissue renewal and specifically in angiogenesis.

In terms of medical implications, the temporal and spatial ablation of uDCs provides a unique experimental model to study this important phase of pregnancy, which will help to understand human infertility where implantation is impaired. Specifically, our results may assist in resolving the limited implantation success of embryos transferred following in vitro fertilization.

Methods

Animals. Eight- to 12-week-old CD11c:DTR transgenic mice (B6.FVB-Tg Itgax-DTR/GFP 57Lan/J) harboring a gene encoding a DTR/GFP fusion protein (17); *Cx$_3$cr1^{gfp}* mice (B6.129P-Cx3cr1tm1Litt/J) harboring a GFP gene in the CX$_3$CR1 locus (18); *Rag2$^{-/-}$* mice (39); and C57BL/6 and BALB/c mice were purchased from Harlan. For semiallogeneic pregnancies, CD11c:DTR C57BL/6 females (H2^b) were mated with BALB/c WT males (H2^d). For syngeneic pregnancies, C57BL/6 CD11c:DTR females were mated with C57BL/6 males. All mice were maintained under specific pathogen–free conditions and handled under protocols approved by the Weizmann Institute Animal Care and Use Committee according to international guidelines.

Depletion of uDCs. Female CD11c:DTR transgenic mice, which express a primate DTR (17), were mated and administered DTx (D-2918; Sigma-Aldrich) on E3.5 of pregnancy (vaginal plug a day after mating: E0.5). DTx was injected i.p. at a dose of 2 ng/g body weight, diluted in PBS for full depletion and 1 ng/g body weight for partial depletion. For local uDC depletion, animals were injected in the myometrium with 20 ng DTx diluted in 30 μl PBS. As control, either CD11c:DTR females were injected with PBS or WT females injected with DTx. On E5.5, mice were sacrificed, and one uterine horn was retrieved for histology and the other flow cytometry analysis, in which uDCs are identified as CD11c^{hi}GFP$^+$ cells.

P4 administration. Subcutaneous injections of 2 mg/ml P4 diluted in sesame oil were administered daily, along with intraperitoneal administration of DTx (2 ng/g body weight), from E3.5 until E5.5 (40).

Artificial decidualization. Females were mated with vasectomized BALB/c mice. On E3.5, females were anesthetized by i.p. injection of 75 mg/kg Ketaset (ketamine; Fort Dodge Animal Health, Wyeth) and 3 mg/kg XYL-M 2% (xylazine; VMD). The upper part of each uterine horn was sutured with a thread. Uteri were collected for analyses 2 days afterward, on E5.5.

Preparation of single-cell suspensions. For isolation of uterine cells including uDCs, either whole uterine horns (of naive and E3.5 females, the latter after washing out embryos for verification of pregnancy) or single ISs (of E4.5 and E5.5 females) were retrieved. ISs were cut from the uteri. Nonimplanted uterine sites were discarded. Since uDCs are virtually absent in the myometrium, ISs were processed along with the myometrium. Tissues were minced into fragments of 1 mm^3 and digested for 35 minutes at 37°C with 1 mg/ml collagenase type IV (Sigma-Aldrich), 0.2 mg/ml DNase (Roche), and 1 mg/ml BSA (Sigma-Aldrich) in PBS with $MgCl_2$ and $CaCl_2$ (Sigma-Aldrich). Then tissues were passed through a mesh and washed in PBS.

Flow cytometry analysis. The staining reagents used in this study included the PE-coupled antibodies against CD8α, I-A^b (MHCII), CD40, CD86, NK1.1, and PE-coupled streptavidin; allophycocyanin-coupled (APC-coupled) anti-CD11c; biotin-conjugated antibodies anti-F4/80 and -CD103 and PerCP-coupled anti-CD11b. Respective isotype antibodies were used for control. Unless otherwise indicated, the reagents were obtained from

eBioscience. Cells were analyzed on FACSCalibur cytometer (BD) using CellQuest software (BD).

Histology. Tissues were fixed in 4% paraformaldehyde for 24 hours, embedded in paraffin, sectioned serially (4 μm), and stained with H&E (Sigma-Aldrich). Photo documentation was performed using an E800 microscope and digital camera DXM 1200 (Nikon). Morphometric analysis of ISs was performed using Image-Pro Plus version 5 software (Media Cybernetics). Tissues were sectioned until the embryo was detected. In cases where the location of the embryo was undetectable (due to embryo loss or upon artificial decidualization), the decidua was cut, and quantifications were performed on sections with the widest decidual diameter.

Immunohistochemistry. Paraffin sections were stained as previously described (41), with the following changes: for uDC detection in CD11c:DTR mice, we used polyclonal biotinylated goat anti-GFP antibodies (ab6658; Abcam). For macrophage detection, we used rat anti-mouse F4/80 antibodies (MCA497GA; Serotec). Antigen retrieval prior to the blocking step was done using 0.1 M trypsin and 0.1 M $CaCl_2$ in 20 mM Tris. Proliferation in the decidua was analyzed with polyclonal rabbit anti-human phospho–histone H3 (Ser10)–R antibodies (sc-8656-R; Santa Cruz Biotechnology Inc.). To determine cell differentiation in the decidua, we used polyclonal rabbit anti-mouse Cx43 antibodies (BD). To test blood vessel functionality, we used biotin-BSA-GdDTPA (MR contrast material; see the following section describing in vivo contrast enhanced MRI stained by fluorescein-labeled avidin [Avidin-FITC; Invitrogen]) as previously described (28). To further test blood vessels, we stained for endothelial cells (using GSL-1 lectin, from *Griffonia simplicifolia*; Sigma-Aldrich) and vascular smooth muscle cells (using anti–α-SMA; Sigma-Aldrich), as previously described (28). For sFlt1 immunostainings, antigen retrieval was performed by microwave heating in pH 6 citrate buffer. An sFlt1-specific antibody was used (36-11000; Zymed, Invitrogen) at 1:100 dilution (42). Photo documentation was performed using Zeiss Axioskop II fluorescent microscope or E800 Nikon microscope.

Two-photon microscopy. Pregnant Cx_3cr1^{gfp} mice (18) were i.v. injected with 200 μl of 0.5 mg/ml TRITC-dextran (150 kDa; Sigma-Aldrich) that was allowed to circulate for 3–5 minutes prior to sacrifice to visualize blood vessels. Uterine tissue was retrieved and immediately visualized by 2-photon microscopy. Two-photon imaging was performed with a Zeiss LSM 510 META NLO microscope equipped with ×20 and ×40 water immersion objectives. A Mai Tai One Box Ti:Sapphire Laser (Spectra Physics, Newport Corp.) was used for 2-photon excitation. Image acquisition was performed using LSM 510 acquisition software. For 2-photon excitation of TRITC-dextran, the laser was tuned to 800 nm, and the emission filter set was 535–590 nm. For excitation of GFP, the laser was tuned to 920 nm, and the emission filter was 500–550 nm.

In vivo contrast-enhanced MRI. MRI was acquired at 4.7T (Bruker) using a whole-body coil. A series of variable-flip-angle precontrast T1-weighted 3D gradient-echo images was acquired to determine the endogenous precontrast R1 (pulse flip angle, 15°, 5°, 30°, 50°, 70°; repetition time [TR], 10 ms; time to echo [TE], 3.6 ms; 2 averages; spectral width, 50,000 Hz; 4 × 4 × 4 cm matrix size, 128 × 128 × 64, zero-filled to 128 × 128 × 128, resulting in a voxel resolution of 313 × 313 × 313 μm [625 μm is the resolution in the third dimension before zero-filling]; total acquisition time per frame,164 seconds; frequency-encoding direction: head-foot). For dynamic contrast-enhanced MRI, 9 mg/mouse (20 g) in 0.2 ml PBS of biotin-BSA-GdDTPA (r = 164 mM^{-1} s^{-1}) was administered via a tail vein catheter and its extravasation monitored over time (MR data were acquired with a pulse flip angle of 15°, and all other parameters as stated above. The first image was acquired 0–164 seconds after administration of the contrast material.) The MRI data allowed quantification of the fBV and the PS (rate of extravasation of contrast material to the interstitial space) on ISs of E5.5, as previously reported (28). In brief, the change in the concentration of the administered MRI contrast material (biotin-BSA-GdDTPA) over time (*Ct*) in the region of interest of the ISs was divided by its concentration in blood (*Cblood*; calculated in the region of interest depicting the vena cava, which was included in the image data set, and extrapolated to time 0). Linear regression of these temporal changes in *Ct*/*Cblood* yielded 2 parameters (the fBV and PS) that characterize vascular development: fBV (= *C0*/*Cblood*) was derived from the concentration of biotin-BSA-GdDTPA in the tissue (*Ct*) extrapolated to the time of administration of the contrast material (*C0*) and divided by its concentration in the vena cava (*Cblood*). *PS* [= (*Ct* – *C0*)/(*Cblood* × *t*)] is the rate of contrast extravasation and accumulation in the tissue derived from the slope of the linear regression of the first 15 minutes after contrast material administration (t = 15).

Fluorescence image analysis. All fluorescence images (of anti–phospho–histone H3 and anti-Cx43, as well as avidin-FITC stainings) were acquired under identical conditions and analyzed using ImageJ software (http://rsbweb.nih.gov/ij/). The fluorescence intensity was measured in absolute counts. The average fluorescence intensity inside the region of interest in the IS was calculated by measuring the ratio of fluorescence signal to the area of region of interest. When probing for vessel density and vessel permeability (after avidin-FITC staining of the MRI contrast material), the areas occupied by clearly resolved blood vessels (attributed to the myometrium or to undecidualized uterine stroma) were masked and excluded from calculation. Fluorescent background was subtracted from each image, where background was measured in the areas without tissue. Vessel density was estimated by determining mean fluorescence at 3 minutes after injection. Vessel permeability was simulated by the change in fluorescence signal intensity between 3 and 15 minutes after injections.

Light microscopy image analysis of immunohistochemical stainings. Quantification of these data (anti-F4/80, anti-sFlt1, anti-GFP, and GSL-1 lectin stainings) was done as previously described (43). In brief, the stained cells/regions were probed and chosen using Adobe Photoshop software, and then the percentage of the stained area from the total IS area was calculated using MacBiophotonics ImageJ software. α-SMA–positive blood vessels were manually counted.

Semiquantitative RT-PCR. Total RNA was extracted from ISs of E5.5 pregnant mice with EZ-RNA Kit (Biological Industries) or from isolated cells with PerfectPure RNA Cell Kit (5 PRIME). Total RNA was reverse transcribed with a mixture of random primers and oligo-dT using a Verso cDNA Kit (Thermo Scientific). cDNA was amplified by PCR using REDTaq ReadyMix (Sigma-Aldrich). We used the following primers: sFlt1 forward, 5′-TTTATCCTGGATCCCAGCAG-3′; sFLT1 reverse, 5′-TGACATGACTTTGTGTGGTAC-3′; TGF-β1 forward, 5′-CTCGGGGCTGCGGCTACTG-3′; TGF-β1 reverse, 5′-GGCGTATCAGTGGGGGTC-3′; actin forward, 5′-CCCCATTGAACATGGCATTGTTAC-3′; actin reverse, 5′-TTGATGTCACGCACGATTTCC-3′.

Statistics. All experiments were repeated 2–3 times, and the number of animals and ISs used for each experiment was indicated accordingly. All data were analyzed using Student's unpaired 2-tailed t test and presented as mean ± SD. A P value of less than 0.05 was considered significant.

Acknowledgments

We thank L. Landsman, E. Berkovitz, N. Nevo, G.M. Damari, Y. Addadi, and R. Krauthgamer for technical help, as well as Y. Melamad and J. Chermesh for animal husbandry. This work was supported by the Israel Science Foundation (ISF), the Kekst Center (S. Jung), the Women's Health Research Center (S. Jung), the Minerva and Israel Science Foundations (M. Neeman), and the Dwek Fund for Biomedical Research (N. Dekel). S. Jung is the incumbent of the Pauline Recanati Career Development Chair; M. Neeman

the incumbent of the Helen and Morris Mauerberger Chair; and N. Dekel the incumbent of the Philip M. Klutznick Professional Chair of Developmental Biology.

Received for publication July 3, 2008, and accepted in revised form September 10, 2008.

Address correspondence to: Steffen Jung, Department of Immunology, Weizmann Institute of Science, Rehovot 76100, Israel. Phone: 972-8-9342787; Fax: 972-8-9342787; E-mail: s.jung@weizmann.ac.il.

Vicki Plaks and Tal Birnberg contributed equally to this work.

1. Rinkenberger, J.L., Cross, J.C., and Werb, Z. 1997. Molecular genetics of implantation in the mouse. *Dev. Genet.* **21**:6–20.
2. Sharkey, A.M., and Smith, S.K. 2003. The endometrium as a cause of implantation failure. *Best Pract. Res. Clin. Obstet. Gynaecol.* **17**:289–307.
3. Matsumoto, H., et al. 2002. Cyclooxygenase-2 differentially directs uterine angiogenesis during implantation in mice. *J. Biol. Chem.* **277**:29260–29267.
4. Pellicer, A., et al. 1999. In vitro fertilization plus preimplantation genetic diagnosis in patients with recurrent miscarriage: an analysis of chromosome abnormalities in human preimplantation embryos. *Fertil. Steril.* **71**:1033–1039.
5. Quenby, S., Farquharson, R.G., Dawood, F., Hughes, A.M., and Topping, J. 2005. Recurrent miscarriage and long-term thrombosis risk: a case-control study. *Hum. Reprod.* **20**:1729–1732.
6. Pulendran, B., et al. 1999. Distinct dendritic cell subsets differentially regulate the class of immune response in vivo. *Proc. Natl. Acad. Sci. U. S. A.* **96**:1036–1041.
7. Hanna, J., et al. 2006. Decidual NK cells regulate key developmental processes at the human fetal-maternal interface. *Nat. Med.* **12**:1065–1074.
8. Croy, B.A., et al. 2003. Uterine natural killer cells: insights into their cellular and molecular biology from mouse modelling. *Reproduction.* **126**:149–160.
9. Ashkar, A.A., Di Santo, J.P., and Croy, B.A. 2000. Interferon gamma contributes to initiation of uterine vascular modification, decidual integrity, and uterine natural killer cell maturation during normal murine pregnancy. *J. Exp. Med.* **192**:259–270.
10. Guimond, M.J., et al. 1997. Absence of natural killer cells during murine pregnancy is associated with reproductive compromise in TgE26 mice. *Biol. Reprod.* **56**:169–179.
11. Kammerer, U. 2005. Antigen-presenting cells in the decidua. *Chem. Immunol. Allergy.* **89**:96–104.
12. Blois, S.M., et al. 2004. Lineage, maturity, and phenotype of uterine murine dendritic cells throughout gestation indicate a protective role in maintaining pregnancy. *Biol. Reprod.* **70**:1018–1023.
13. Steinman, R.M., Hawiger, D., and Nussenzweig, M.C. 2003. Tolerogenic dendritic cells. *Annu. Rev. Immunol.* **21**:685–711.
14. Mowat, A.M. 2003. Anatomical basis of tolerance and immunity to intestinal antigens. *Nat. Rev. Immunol.* **3**:331–341.
15. Laskarin, G., et al. 2007. Antigen-presenting cells and materno-fetal tolerance: an emerging role for dendritic cells. *Am. J. Reprod. Immunol.* **58**:255–267.
16. Zarnani, A.H., Moazzeni, S.M., Shokri, F., Salehnia, M., and Jeddi-Tehrani, M. 2007. Kinetics of murine decidual dendritic cells. *Reproduction.* **133**:275–283.
17. Jung, S., et al. 2002. In vivo depletion of CD11c(+) dendritic cells abrogates priming of CD8(+) T cells by exogenous cell-associated antigens. *Immunity.* **17**:211–220.
18. Jung, S., et al. 2000. Analysis of fractalkine receptor CX(3)CR1 function by targeted deletion and green fluorescent protein reporter gene insertion. *Mol. Cell. Biol.* **20**:4106–4114.
19. Austyn, J.M., and Gordon, S. 1981. F4/80, a monoclonal antibody directed specifically against the mouse macrophage. *Eur. J. Immunol.* **11**:805–815.
20. Turnbull, E.L., Yrlid, U., Jenkins, C.D., and Macpherson, G.G. 2005. Intestinal dendritic cell subsets: differential effects of systemic TLR4 stimulation on migratory fate and activation in vivo. *J. Immunol.* **174**:1374–1384.
21. Shortman, K., and Naik, S.H. 2007. Steady-state and inflammatory dendritic-cell development. *Nat. Rev. Immunol.* **7**:19–30.
22. Steinbrink, K., Wolfl, M., Jonuleit, H., Knop, J., and Enk, A.H. 1997. Induction of tolerance by IL-10-treated dendritic cells. *J. Immunol.* **159**:4772–4780.
23. Blois, S.M., et al. 2007. Dendritic cells: key to fetal tolerance? *Biol. Reprod.* **77**:590–598.
24. Turner, C.D., and Bagnara, J.T. 1976. Biological effects of the ovarian hormones. *General endocrinology.* 6th edition. Harcourt College Publishers. Philadelphia, Pennsylvania, USA. 488–489.
25. Bulletti, C., and de Ziegler, D. 2006. Uterine contractility and embryo implantation. *Curr. Opin. Obstet. Gynecol.* **18**:473–484.
26. Baek, S.H., et al. 2002. Exchange of N-CoR corepressor and Tip60 coactivator complexes links gene expression by NF-kappaB and beta-amyloid precursor protein. *Cell.* **110**:55–67.
27. Winterhager, E., Grummer, R., Jahn, E., Willecke, K., and Traub, O. 1993. Spatial and temporal expression of connexin26 and connexin43 in rat endometrium during trophoblast invasion. *Dev. Biol.* **157**:399–409.
28. Plaks, V., Kalchenko, V., Dekel, N., and Neeman, M. 2006. MRI analysis of angiogenesis during mouse embryo implantation. *Magn. Reson. Med.* **55**:1013–1022.
29. Olsson, A.K., Dimberg, A., Kreuger, J., and Claesson-Welsh, L. 2006. VEGF receptor signalling - in control of vascular function. *Nat. Rev. Mol. Cell Biol.* **7**:359–371.
30. Godkin, J.D., and Dore, J.J. 1998. Transforming growth factor beta and the endometrium. *Rev. Reprod.* **3**:1–6.
31. Erlebacher, A., Vencato, D., Price, K.A., Zhang, D., and Glimcher, L.H. 2007. Constraints in antigen presentation severely restrict T cell recognition of the allogeneic fetus. *J. Clin. Invest.* **117**:1399–1411.
32. Baulieu, E.E. 1989. Contragestion and other clinical applications of RU 486, an antiprogesterone at the receptor. *Science.* **245**:1351–1357.
33. Aschenbrenner, K., et al. 2007. Selection of Foxp3+ regulatory T cells specific for self antigen expressed and presented by Aire+ medullary thymic epithelial cells. *Nat. Immunol.* **8**:351–358.
34. Torry, D.S., et al. 2007. Angiogenesis in implantation. *J. Assist. Reprod. Genet.* **24**:303–315.
35. Halder, J.B., et al. 2000. Differential expression of VEGF isoforms and VEGF(164)-specific receptor neuropilin-1 in the mouse uterus suggests a role for VEGF(164) in vascular permeability and angiogenesis during implantation. *Genesis.* **26**:213–224.
36. Chakraborty, I., Das, S.K., and Dey, S.K. 1995. Differential expression of vascular endothelial growth factor and its receptor mRNAs in the mouse uterus around the time of implantation. *J. Endocrinol.* **147**:339–352.
37. Holderfield, M.T., and Hughes, C.C. 2008. Crosstalk between vascular endothelial growth factor, notch, and transforming growth factor-beta in vascular morphogenesis. *Circ. Res.* **102**:637–652.
38. Machens, H.G., et al. 2003. Angiogenic effects of injected VEGF165 and sVEGFR-1 (sFLT-1) in a rat flap model. *J. Surg. Res.* **111**:136–142.
39. Shinkai, Y., et al. 1993. Restoration of T cell development in RAG-2-deficient mice by functional TCR transgenes. *Science.* **259**:822–825.
40. Lim, H., Ma, L., Ma, W.G., Maas, R.L., and Dey, S.K. 1999. Hoxa-10 regulates uterine stromal cell responsiveness to progesterone during implantation and decidualization in the mouse. *Mol. Endocrinol.* **13**:1005–1017.
41. Sapoznikov, A., et al. 2007. Organ-dependent in vivo priming of naive CD4+, but not CD8+, T cells by plasmacytoid dendritic cells. *J. Exp. Med.* **204**:1923–1933.
42. Sela, S., et al. 2008. A novel human-specific soluble vascular endothelial growth factor receptor 1: cell type-specific splicing and implications to vascular endothelial growth factor homeostasis and preeclampsia. *Circ. Res.* **102**:1566–1574.
43. Preise, D., et al. 2008. Systemic antitumor protection by vascular-targeted photodynamic therapy involves cellular and humoral immunity. *Cancer Immunol. Immunother.* Online publication ahead of print. doi:10.1007/s00262-008-0527-0.